OPTICAL MODEL FOR THIN-FILM PHOTOVOLTAIC DEVICES WITH LARGE SURFACE TEXTURES AT THE FRONT SIDE

Benjamin Lipovšek, Janez Krč, Marko Topič

University of Ljubljana, Faculty of Electrical Engineering, Ljubljana, Slovenia

Key words: Thin-film silicon solar cells, optical modelling, textured glass, ray tracing, transfer matrix formalism

Abstract: An optical model for simulation of thin-film photovoltaic devices with thick surface-textured front components is presented. The model is based on the combination of incoherent geometric optics and coherent wave optics analysis, which are employed separately to simulate light propagation through the front textured component and the bottom flat thin-film component of the device, respectively. The verified model is implemented into the optical simulator CROWM, which is employed to study the light-trapping potential of the front surface-textured protective glass in thin-film photovoltaic modules. The results show that the texturisation in the range of millimetres significantly improves the quantum efficiency of the PV module, which results in 14.3 % higher J_{SC} compared to the conventional module with flat protective glass.

Optični model za tankoplastne fotonapetostne strukture z velikimi površinskimi teksturami na sprednji strani

Kjučne besede: tankoplastne silicijeve sončne celice, optično modeliranje, teksturirano steklo, metoda sledenja žarkov, metoda prenosnih matrik

Izvleček: V članku je predstavljen optični model za simulacijo tankoplastnih sončnih celic in fotonapetostnih modulov z velikimi površinskimi teksturami na sprednji strani strukture. Model temelji na kombinaciji nekoherentne geometrijske optike in koherentne valovne optike. Prvo uporabljamo za simulacijo potovanja svetlobe skozi sprednjo teksturirano komponento strukture, drugo pa za simulacijo spodnje tankoplastne strukture. Verificirani optični model je implementiran v optičnem simulatorju CROWM ("Combined Ray Optics / Wave Optics Numerical Model"), s katerim preučujemo potencial teksturiranega zaščitnega stekla za izboljšanje svetlobnega ujetja v tankoplastnih fotonapetostnih modulih. Rezultati kažejo, da površinska teksturizacija sprednjega stekla v milimetrskem območju bistveno izboljšuje kvantni izkoristek modula, kar se odraža v 14.3 % višji kratkostični gostoti toka v primerjavi s konvencionalnim modulom z gladkim sprednjim steklom.

1. Introduction

Optical modelling and simulation of optoelectronic devices such as solar cells and photovoltaic modules (PV devices) presents a powerful tool for design and optimisation of the device structures and their optical performances /1/. Simulations allow efficient and inexpensive analysis of numerous factors which influence the performance and also offer a predictive power which can be used in the design of novel device concepts. Thin-film PV devices, which are the subject of this paper, are multilayer structures consisting of semi-transparent thin and thick layers /2/. The thickness of the thin layers (semiconductor layers, transparent conductive oxide (TCO) contacts etc.) is in the range of nanometres and micrometres, whereas the thickness of the front or back substrate is in the range of millimetres. The level of interference fringes observed in the measured wavelength-dependent reflection and transmission spectra of thin-film solar cells indicate that coherent light propagation takes place within the thin layers of the device, as opposed to incoherent propagation observed in the thick transparent substrates /3/. Further on, textured interfaces or nanoparticles are employed in the structures to scatter the light and thus increase the optical paths and the absorption of light in the thin layers /4, 5/. The lateral and vertical dimensions of the texture features can be either in the range of nanometres, as is typically the case at internal interfaces, or in the range of microns or even millimetres in the case of surface-textured glass substrates /6/. Texturisation of solar cells introduces additional complexity that has to be taken into account in optical modelling and simulation of such structures.

Over the years, different optical models have been developed to combine coherent and incoherent propagation of light in thin and thick layers, respectively, and to tackle light scattering effects at nano-textured interfaces inside the solar cell structures /7–13/. However, most of these models cannot be easily applied to simulation of thin-film solar cells with thick surface-textured front components, such as glass substrates with large surface textures, due to several drawbacks. First, most of the models are designed primarily for one specific type of light propagation (coherent or incoherent) and don't allow for combination of both. Second, the limited dimensions of the simulation domain would make most of the models unfeasible for larger structures, such as thick glass layers. And third, the models are often limited to one dimension and don't allow an exact morphology of the surface texture to be specified.

In this paper, we present an optical model which combines light scattering at large textures (from a few microns to a few millimetres) located at the front surface of the PV device with coherent propagation and absorption of the scattered waves in the thin layers of the device. The model is based on the combination of incoherent two-dimensional ray tracing (geometric optics) /13/, which is employed to analyse the

thick front substrate, and coherent one-dimensional transfer matrix formalism (wave optics) /14/, which is used for the bottom thin-film component of the device. The development of the model (i.e. the mathematical procedures and the physical background) will be described in detail in Section 2, and verification of the model with other verified optical simulators will be presented in the first part of Section 3. Finally, the developed optical model will be employed to simulate *a*-Si:H PV modules with thick protective glass at the front side, including large front surface textures. The beneficial effects of the texturisation with respect to an improved light trapping within the solar cells will be demonstrated.

2. Development of the optical model

The developed optical model is based on the combination of two fundamentally different numerical methods for the analysis of light propagation, which are applied separately to different parts of the simulated PV device (Fig. 1). The front part of the device (i.e. the incident medium and the thick surface-textured front layer) is treated by means of two-dimensional ray tracing /13/, where geometric optics approach is used to determine the angles and the intensities of light rays reflected or transmitted at the front textured interface. Within the thick front layer, completely incoherent propagation of light rays without any interference effects is assumed, which is justified since both the thickness of the front layer and the dimensions of the texture features are much larger (> 10 μm) than the effective wavelength of light. The surface texture is assumed to be periodic or quasi-periodic, in which case one period of the texture is included in the simulation while periodic boundary conditions are applied to the lateral borders. The bottom, thin-film part of the PV device (i.e. the flat thin-film multilayer stack), on the other hand, is analysed by means of the transfer matrix formalism /14/. Transfer matrix formalism is a one-dimensional approach from wave optics which allows the analysis of fully coherent light propagation through the thin-film system under arbitrary incident angles, taking into account constructive and destructive interference of the forward and backward propagating waves. In the following sections, both approaches – geometric ray tracing and thin-film wave optics – and their combination into one efficient optical model are described in detail.

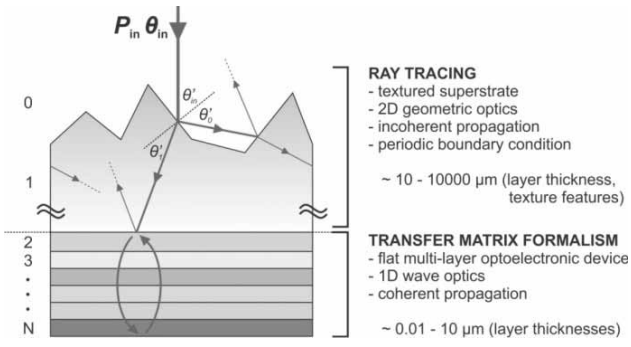

Fig. 1: The principle of the combined optical model – separation of the analysed structure into the top and bottom components, employing different modelling approaches for each case.

2.1 Ray tracing

The incident illumination in the form of a plane wave is applied from the incident medium at the top border of the simulation domain, following an arbitrary incident angle. The full spectrum of the incident illumination is discretised into a number of monochromatic spectral components, and the simulation then takes place separately for each component (wavelength). Furthermore, the incident illumination is divided into the transverse-electric (TE) and the transverse-magnetic (TM) polarisation relative to the horizontal plane parallel to the interfaces in the thin-film stack. An arbitrary power ratio between the TE and TM polarised incident light can be chosen. All the calculations are performed separately for the TE and TM parts, and they are only combined at the end to produce the final results (see Section 2.3).

Simulation for a single monochromatic spectral component (wavelength λ) begins by dividing the total power of the component among a number of coherent parallel incident rays (separately for TE and TM), which are distributed evenly across the width of the simulation domain (in Fig. 1, only one incident ray is plotted schematically). The basic quantity that is used to define the light rays/waves propagating through the simulated structure is the electric field *E*, which is represented as a complex number (magnitude and phase). The electric fields corresponding to the incident rays are initialised according to Eq. 1,

$$E_{in} = \sqrt{\Re\left\{\frac{2\eta_0}{n_{in}}\right\} \cdot P_{in}} \tag{1}$$

Where P_{in} represents the time-averaged incident power per unit area of the ray, η_0 is the characteristic impedance in vacuum ($\eta_0 = \sqrt{\mu_0/\varepsilon_0}$), and n_{in} is the refractive index of the incident medium (this is typically air for simulation of terrestrial solar cells). In general, the refractive index is a complex value composed of the real part n_{re} and imaginary part k (also called the extinction coefficient), so that $n = n_{re} - j \cdot k$ (j is the imaginary unit). Zero phase is assumed for all the electric fields of the incident rays.

Once the electric fields are initialised at the top border of the simulation domain, each ray is propagating through the incident medium in a straight line following the propagation angle q_{in} until it either (i) impinges upon the textured surface of the thick front layer of the device or (ii) reaches one of the lateral borders of the simulation domain, in which case it simply reappears at the opposite border according to the periodic boundary condition. In the first case, the magnitude and the phase of the electric fields are first corrected according to Eq. 2, where λ represents the wavelength (in vacuum) of the analysed spectral component and *d* is the distance that the ray travelled through the incident medium until reaching the interface point.

$$E = E_{in} \cdot \exp\left(\frac{-i \cdot 2\pi \cdot n_{in} \cdot d}{\lambda}\right) \quad (2)$$

To determine the reflected and the transmitted components of the electric field from the textured surface, the incident angle θ_{in}, the angle of reflection θ_0, and the angle of refraction θ_1' are first calculated. These are all relative angles with respect to the local inclination of the texture at the point where the ray impinges upon the surface. While the relative angle of the reflected ray is the same as the incident angle ($\theta_0' = \theta_{in}'$), the angle of the refracted (transmitted) ray θ_1' is defined according to Snell's law, as shown in Eq. 3 /15/,

$$n_{in} \cdot \sin\theta_{in}' = n_1 \cdot \sin\theta_1' \quad (3)$$

Where n_1 represents the complex refractive index of the thick front layer. In general, the calculated angle θ_1' is also a complex value, and thus only the real part is taken to define the propagating angle of the transmitted ray. The Fresnel coefficients which determine the reflectance and the transmittance of the electric fields for the TE and TM polarised rays are then calculated according to Eq. 4 /15/.

$$r^{TE} = \frac{n_{in} \cdot \cos\theta_{in}' - n_1 \cdot \cos\theta_1'}{n_{in} \cdot \cos\theta_{in}' + n_1 \cdot \cos\theta_1'}$$

$$t^{TE} = 1 + r^{TE} = \frac{2 \cdot n_{in} \cdot \cos\theta_{in}'}{n_{in} \cdot \cos\theta_{in}' + n_1 \cdot \cos\theta_1'}$$

$$r^{TM} = \frac{n_{in} \cdot \cos\theta_1' - n_1 \cdot \cos\theta_{in}'}{n_{in} \cdot \cos\theta_1' + n_1 \cdot \cos\theta_{in}'}$$

$$t^{TM} = \left(1 + r^{TM}\right) \cdot \frac{\cos\theta_{in}'}{\cos\theta_1'} = \frac{2 \cdot n_{in} \cdot \cos\theta_{in}'}{n_{in} \cdot \cos\theta_1' + n_1 \cdot \cos\theta_{in}'} \quad (4)$$

The reflected and the transmitted rays are then propagating further through the structure following a straight trajectory defined by the new propagating angles. The electric fields of the rays are obeying Eq. 2, where E_{in} and n_{in} are replaced with $r \cdot E$ and n_{in} (reflected ray) or $t \cdot E$ and n_1 (transmitted ray). This propagation takes place until one of the following happens: (i) the ray once again impinges upon the textured interface, in which case the above procedure (Eq. 3 – 4) is repeated, (ii) the ray reaches the top border of the simulation domain and thus escapes out of the structure, contributing to the total reflectance, or (iii) the ray reaches the bottom border of the thick front layer and thus enters the bottom thin-film component of the device. In the latter case, the outgoing ray represents the incident illumination for the bottom multilayer stack which is treated by means of the transfer matrix formalism.

2.2 Transfer matrix formalism

The transfer matrix formalism is a widely established one-dimensional method for simulating the propagation of electromagnetic waves through a thin-film multilayer stack with flat parallel interfaces /14/. The method is based on the distribution of the wave propagating through the medium under an arbitrary angle into two components – the transverse component which is traveling perpendicular to the flat interfaces, and the parallel component traveling in parallel along the interfaces. The method then focuses on the propagation of the transverse wave components, since only these waves are able to interact constructively or destructively with each other, whereas the information about the full wave (transverse plus parallel) is retained within the propagating angles.

The incident waves for the bottom thin-film component of the simulated device are generated from the downward-traveling rays coming from the top component. The transition takes place just before the interface between the thick front layer (layer 1 in Fig. 1) and the first thin layer in the thin-film stack (layer 2 in Fig. 1). The transverse electric fields of the incident waves are thus calculated from the electric fields of the outgoing rays according to Eq. 5, taking into account the propagating angle q_1.

$$E_{T,in}^{TE} = E^{TE}$$

$$E_{T,in}^{TM} = E^{TM} \cdot \cos\theta_1 \quad (5)$$

Assuming that there is a total of *N–2* thin layers in the multilayer stack, we can calculate the complex propagation angle θ_i, the phase thickness δ_i, and the transverse impedance $\eta_{T,i}$ for each layer in the stack (*i*) according to Eq. 6 – 8 /15/, where d_i represents the thickness of the layer. Furthermore, for each interface (*i*) in the thin-film multilayer stack, we can determine the transverse Fresnel coefficients given by Eq. 9. The nomenclature is chosen so that the *i*-th interface is located between the *i*-th and the (*i*+1)-th layer.

$$\theta_i = \sin^{-1}\left(\frac{n_1}{n_i} \cdot \sin\theta_1\right) \qquad i = 2, 3, \ldots, N \quad (6)$$

$$\delta_i = \frac{2\pi \cdot n_i \cdot d_i \cdot \cos\theta_i}{\lambda} \qquad i = 2, 3, \ldots, N-1 \quad (7)$$

$$\eta_{T,i}^{TE} = \frac{\eta_0}{n_i \cdot \cos\theta_i}$$

$$\eta_{T,i}^{TM} = \frac{\eta_0 \cdot \cos\theta_i}{n_i} \qquad i = 1, 2, \ldots, N \quad (8)$$

$$r_{T,i}^{TE} = \frac{n_i \cdot \cos\theta_i - n_{i+1} \cdot \cos\theta_{i+1}}{n_i \cdot \cos\theta_i + n_{i+1} \cdot \cos\theta_{i+1}}$$

$$t_{T,i}^{TE} = 1 + r_{T,i}^{TE} = \frac{2 \cdot n_i \cdot \cos\theta_i}{n_i \cdot \cos\theta_i + n_{i+1} \cdot \cos\theta_{i+1}}$$

$$r_{T,i}^{TM} = \frac{n_i \cdot \cos\theta_{i+1} - n_{i+1} \cdot \cos\theta_i}{n_i \cdot \cos\theta_{i+1} + n_{i+1} \cdot \cos\theta_i}$$

$$t_{T,i}^{TM} = 1 + r_{T,i}^{TM} = \frac{2 \cdot n_i \cdot \cos\theta_{i+1}}{n_i \cdot \cos\theta_{i+1} + n_{i+1} \cdot \cos\theta_i} \qquad i = 1, 2, \ldots, N-1 \quad (9)$$

The simulation of wave propagation through the thin-film stack consists of two steps. First, the reflected and the transmitted fields of the whole stack are calculated by applying the matching and the propagation matrices of the interfaces and the layers, respectively. The matching matrices *M* give the relation between the forward and the backward propagating transverse electric fields at each side of an interface (Eq. 10), whereas the propagation matrices *P* define how the fields are affected by propagating through

a layer (Eq. 11), where indices *a* and *b* stand for the top and bottom border of the layer.

$$\begin{bmatrix} E^+_{T,i} \\ E^-_{T,i} \end{bmatrix} = \frac{1}{t_{T,i}} \begin{bmatrix} 1 & r_{T,i} \\ r_{T,i} & 1 \end{bmatrix} \cdot \begin{bmatrix} E^+_{T,i+1} \\ E^-_{T,i+1} \end{bmatrix} = [M_i] \cdot \begin{bmatrix} E^+_{T,i+1} \\ E^-_{T,i+1} \end{bmatrix} \quad (10)$$

$$\begin{bmatrix} E^+_{T,ia} \\ E^-_{T,ia} \end{bmatrix} = \begin{bmatrix} \exp(j \cdot \delta_i) & 0 \\ 0 & \exp(-j \cdot \delta_i) \end{bmatrix} \cdot \begin{bmatrix} E^+_{T,ib} \\ E^-_{T,ib} \end{bmatrix} = [P_i] \cdot \begin{bmatrix} E^+_{T,ib} \\ E^-_{T,ib} \end{bmatrix} \quad (11)$$

The reflected and the transmitted fields of the stack are obtained by multiplying the matrices from the incident medium (thick front layer) to the medium in transmission, as shown in Eq. 12:

$$\begin{bmatrix} E_{T,in} \\ E_{T,reflected} \end{bmatrix} = [M_1] \cdot [P_2] \cdot [M_2] \cdot \ldots \cdot [P_{N-1}] \cdot [M_{N-1}] \cdot \begin{bmatrix} E_{T,transmitted} \\ 0 \end{bmatrix} \quad (12)$$

In the second step, the total transverse electric and magnetic fields are calculated at each interface throughout the device. This is important to determine the absorptions within the individual layers of the thin-film stack. The fields at the first interface are calculated from the incident and the reflected electric fields according to Eq. 13, and then the fields at the following interfaces are determined by applying the propagation matrix in the recursions shown in Eq. 14.

$$\begin{bmatrix} E_{T,1} \\ H_{T,1} \end{bmatrix} = \begin{bmatrix} E_{T,in} + E_{T,reflected} \\ \frac{1}{\eta_1}\left(E_{T,in} - E_{T,reflected}\right) \end{bmatrix} \quad (13)$$

$$\begin{bmatrix} E_{T,i} \\ H_{T,i} \end{bmatrix} = \begin{bmatrix} \cos(\delta_i) & -j\eta_i \sin(\delta_i) \\ -j\frac{1}{\eta_i}\sin(\delta_i) & \cos(\delta_i) \end{bmatrix} \cdot \begin{bmatrix} E_{T,i-1} \\ H_{T,i-1} \end{bmatrix}$$

$$i = 2, 3, \ldots, N-1 \quad (14)$$

Finally, the time-averaged power per unit area entering the *i*-th layer as well as the power lost within the layer can be determined from the Poynting vector according to Eq. 15.

$$P_i = \frac{1}{2}\Re\left\{E_{T,i-1} \cdot H^*_{T,i-1}\right\} \qquad i = 2, 3, \ldots, N$$
$$A_i = P_i - P_{i+1} \qquad i = 2, 3, \ldots, N-1 \quad (15)$$

The summation of the power losses calculated for each ray entering the thin-film multilayer stack relative to the total incident power gives the total absorptance within each layer of the simulated optoelectronic device, whereas the power of the transmitted waves is contributing to the total transmittance.

2.3 Combination of ray tracing and transfer matrix formalism

Both optical models, ray tracing in the top part (layers 0 and 1) and transfer matrix formalism in the bottom part of the structure (layers 2 – N), are then coupled iteratively at the interface between the thick front layer and the bottom multilayer stack. Rays reaching the interface from the front layer are injected as waves into the thin-film stack, whereas the waves coming back from the thin-film stack re-enter the front layer as backward-traveling rays. Simulation concludes once almost all of the light (according to some pre-defined threshold) has either escaped out of the structure (contributing to the total reflectance or the total transmittance) or has been absorbed in the device (contributing to the absorptance within the layers). The reflectance, the transmittance, and the absorptance are defined as the ratios of the reflected, transmitted and absorbed power relative to the total incident power, respectively, as defined in Eq. 16.

$$R_{tot} = \frac{P_R}{P_{in}} \qquad T_{tot} = \frac{P_T}{P_{in}} \qquad A = \frac{P_A}{P_{in}} \quad (16)$$

The primary input parameters of the developed optical model are the geometry and the physical properties of the simulated device, in particular (i) the description of the front surface texture, (ii) the layer thicknesses, (iii) the wavelength-dependent complex refractive indices of the materials, and (iv) the lateral boundaries (period) of the simulation domain, and the properties of the incident illumination, in particular (i) the propagation angle q_{in}, (ii) the spectral (wavelength) range, (iii) the total time-averaged power per unit area P_{in} for each spectral component, and (iv) the polarisation of light (TE and TM components with respect to the lateral plane of the device structure). The primary output parameters are (i) the total reflectance, (ii) the total transmittance of the device, and (iii) the absorptance within the individual layers of the structure.

The combined optical model was implemented in a computer simulator entitled CROWM (Combined Ray Optics / Wave Optics Numerical Model), which runs on a personal computer and allows for many advanced features primarily related to automatic optimisation of PV devices with respect to the desired output characteristics.

3. Simulation results

To demonstrate the applicability of the CROWM simulator based on the developed combined optical model to the analysis of thin-film PV devices, thin-film amorphous silicon (*a*-Si:H) solar cells encapsulated in PV modules with flat and textured front glass surfaces were simulated. The basic solar cell structure without the front component (encapsulation) which was used in all the simulations is constructed as follows: front SnO_2:In (ITO) transparent conductive oxide (TCO) (70 nm), *p*-*a*-SiC:H layer (10 nm), *i*-*a*-Si:H absorber (250 nm), *n*-*a*-Si:H layer (20 nm), ZnO TCO (80 nm), Ag (300 nm)/substrate. The cell is in the so-called substrate configuration with the non-transparent substrate located at the back side. In all the simulations, realistic refractive indices of all the layers comprising the solar cell were employed /12/.

3.1 Verification of the simulator

To verify the CROWM simulator, the simulation results were compared to the results obtained by other verified optical

simulators for the analysis of thin-film PV devices. Besides the accuracy of the results, the speed of the simulation which represents an important indicator for efficient simulation and optimisation of the analysed structures was also investigated and compared between the models, using a high-end personal computer for all the simulations.

A perfectly flat *a*-Si:H solar cell with 1 mm thick glass layer at the front side (see inset in Fig. 2) was simulated by means of the CROWM and Sun*Shine* optical simulators /7/. The Sun*Shine* is a verified and well-established one-dimensional semi-coherent optical simulator based on the scalar scattering theory, applicable to nano-textured interfaces. The external quantum efficiency (*QE*) of the solar cell simulated by both optical models in the wavelength range of 350 – 800 nm is shown in Fig. 2. The *QE* was calculated as the absorptance in the *i*-*a*-Si:H layer, assuming ideal extraction of the charge carriers /7/. It can be observed that identical results are obtained in both cases (curves are overlapping). The simulation times are also similar for both optical models and result in less than 20 seconds.

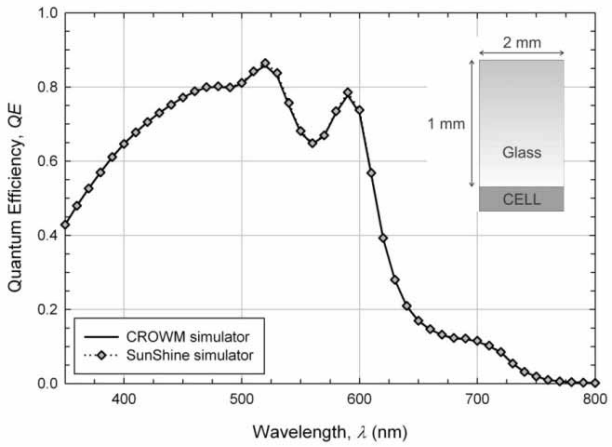

Fig. 2: Comparison of the quantum efficiencies simulated by means of the CROWM (full line) and SunShine optical simulators (dotted line with symbols) for the a-Si:H solar cell with flat front component (inset).

An *a*-Si:H solar cell with surface-textured glass layer at the front side was simulated by means of the CROWM and FEMOS-2D optical simulators /8/. FEMOS-2D is a verified fully-coherent two-dimensional simulator based on rigorous solving of electromagnetic wave equations using the finite element method (FEM). However, since FEMOS-2D was not designed for simulation of layers thicker than 10 µm, the dimensions of the front glass were scaled down to comply with this limitation. Thus, a 10 µm thick glass layer with a periodic triangular surface texture with the period P = 10 µm and amplitude h = 3 µm was employed in the simulations (see inset in Fig. 3). The *QE* results obtained by both simulators are shown in Fig. 3. Good agreement between the results can generally be observed, although slightly lower values are obtained by the FEMOS-2D simulator. These discrepancies can mostly be attributed to the relatively coarse non-adaptive triangular mesh used in FEMOS-2D (10 nm element size), which was required due to the relatively large simulation domain. Despite the coarser grid, however, the FEMOS-2D simulation lasted for more than one day, whereas the simulation by the developed CROWM simulator was completed in less than half an hour (time ratio of more than 1:50). Therefore, CROWM shows great potential for efficient simulation and optimisation of solar cells with thick surface-textured front components with large textures, which can become unwieldy for the conventional numerical methods such as FEM.

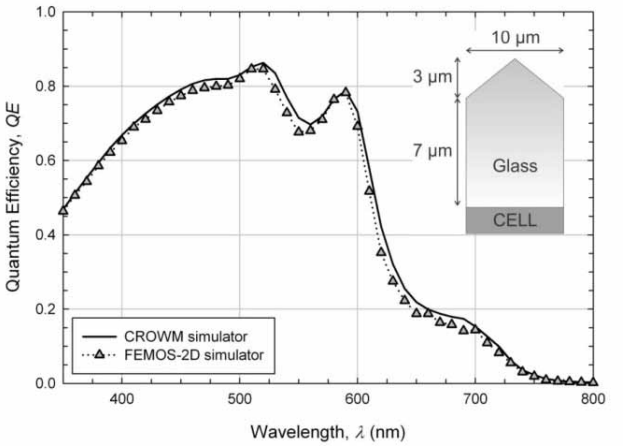

Fig. 3: Comparison of the quantum efficiencies simulated by means of the CROWM (full line) and FEMOS-2D optical simulators (dotted line with symbols) for the a-Si:H solar cell with surface-textured front component (inset).

3.2 Simulation of thin-film *a*-Si:H PV devices with thick textured protective glass

When the solar cells are encapsulated in PV modules, they are typically covered with about 100 µm of ethylene-vinyl acetate (EVA) foil, serving as an air-tight seal, and 4 mm of flat protective glass /1/. From the optical point of view, this additional component at the front side of the solar cell represents an optical barrier for the light entering the structure. Despite the better refractive index grading which is assured in this system (the refractive indices of glass and EVA are between those of air and ITO), incoherent properties of the thick glass and EVA foil do not lead to improved, but rather worse anti-reflecting properties compared to the initial solar cell structure. Simulations with the developed optical model show that the initial non-encapsulated *a*-Si:H solar cell illuminated with the standard AM1.5 solar spectrum exhibits the short-circuit current density J_{SC} = 12.43 mA/cm^2. After encapsulation, however, the additional reflections at the air/glass and EVA/TCO interfaces as well as the parasitic absorption within glass and EVA foil reduce J_{SC} to 11.51 mA/cm^2, which is a 7.4 % decrease compared to the non-encapsulated solar cell.

To improve the performance of thin-film solar cells, light trapping within the thin absorber layers of the device needs

to be assured. Improved light trapping in state-of-the-art *a*-Si:H solar cells is typically achieved by nano-textured internal interfaces, which introduce efficient scattering of the light propagating through the device /4/. Besides the internal interfaces, however, light scattering can also be achieved by the front protective glass. For this purpose, texturisation in form of spikes or grooves needs to be realised for example on the surface of the protective glass sheet /6/. This has two effects for the incident light rays impinging perpendicularly upon the textured surface. First, the rays transmitted through the air/glass interface are refracted into larger incident angles, which results in prolonged optical paths through the absorber layers of the cell and thus an increased J_{SC}. And second, the rays reflected from the textured air/glass interface have a chance to impinge upon the interface and enter the device once more, which results in a decreased total reflectance from the solar module.

To demonstrate the light-trapping potential of the front protective glass in solar modules, flat *a*-Si:H solar cells covered with 100 µm of EVA foil and 4 mm of flat and surface-textured glass are simulated by means of the CROWM simulator. The refractive indices of EVA and glass are assumed to be the same in these simulations, and thus the reflection/refraction effects at the glass/EVA interface can be neglected. In the case of texturing, quasi random triangular one-dimensional texturisation with the period of 2 mm and peak-to-peak amplitude of 1 mm is applied to the top of the front glass, as shown in Fig. 4a. A more detailed plot of the textured surface of the glass sheet is presented in Fig. 4b.

(a)

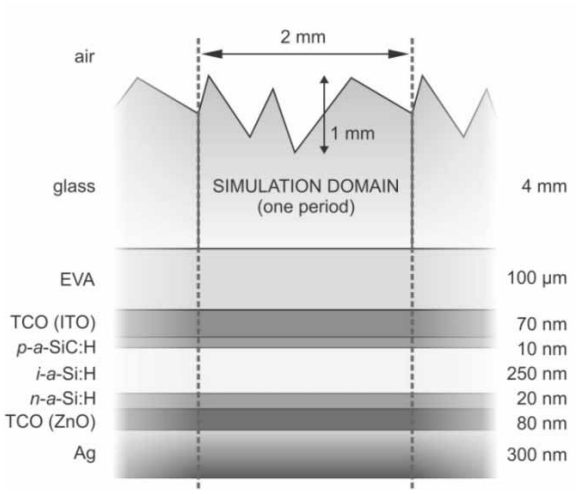

(b)

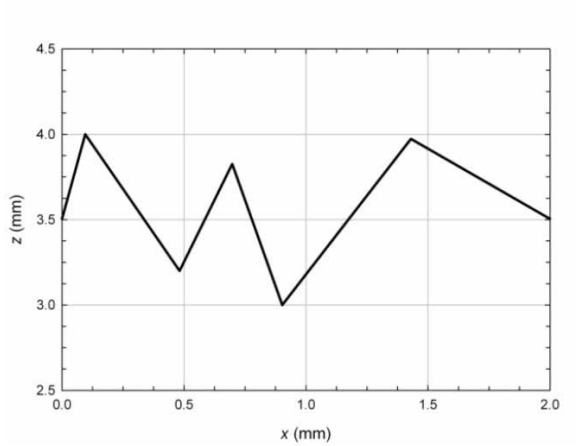

Fig. 4: Structure of the a-Si:H solar cell encapsulated by 100 µm thick film of EVA foil and 4 mm thick surface-textured glass (a). The profile of the surface texture of the glass sheet is also shown (b).

The simulated trajectories of ray propagation through the surface-textured glass prior to reaching the thin-film *a*-Si:H solar cell are plotted in Fig. 5a. The rays impinging perpendicularly upon the textured surface (thick vertical lines at

(a)

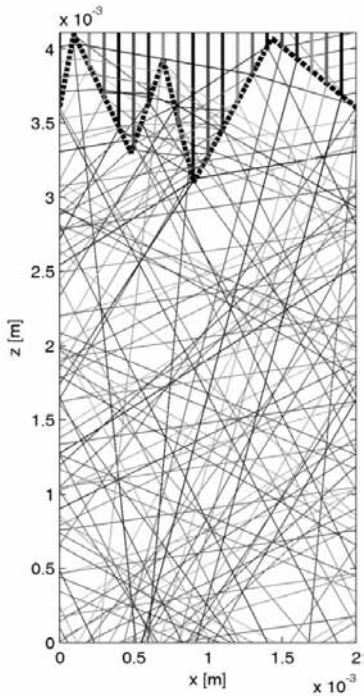

(b)

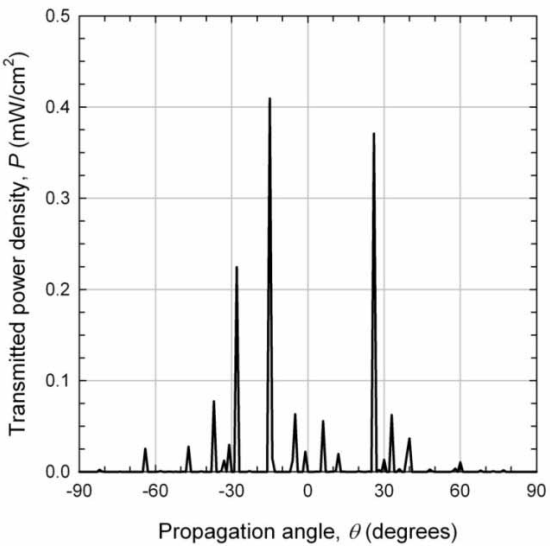

Fig. 5: Ray propagation through the surface-textured glass (a) and angular distribution of the transmitted ray power at the interface with the front TCO of the solar cell (b).

the top of the figure) are refracted into large propagating angles, and multiple reflection/refraction events can also be observed, leading to lower reflectance. Simulations show that in the wavelength range of 350 – 900 nm, only 0.4 % of the total incident power is reflected by the textured air/glass interface, whereas in the case of flat glass, this value is more than ten times larger (4.4 %). The angular distribution of the transmitted ray power at the bottom border (EVA/TCO) of the front protective layer is presented in Fig. 5b. The figure indicates that the majority of the transmitted ray power is impinging upon the underlying solar cell with incident angles larger than 20 degrees, which will result in longer effective optical paths through the thin absorber layers and thus an increased efficiency of the solar cell.

The simulated quantum efficiencies of thin-film *a*-Si:H solar cells encapsulated with flat and surface-textured glass are presented in Fig. 6. A substantial increase in *QE* over the entire wavelength range can be observed for the surface-textured module, which can be attributed directly to the enhanced light trapping achieved by the texturisation of glass. Simulations show that J_{SC} = 13.16 mA/cm^2 can be achieved in this case, which is 14.3 % higher than J_{SC} of the flat module (11.51 mA/cm^2), and 5.9 % higher than J_{SC} of the non-encapsulated cell (12.43 mA/cm^2). These results indicate that surface texturisation of the protective glass not only compensates for the negative effects of encapsulation, but further improves the short-circuit current density of the cell and thus the efficiency of the solar module. The challenge remains, however, to further optimise the morphology of the surface texturisation in order to achieve the highest possible efficiency of the photovoltaic device and to test the effect also for solar cells with nano-textured internal interfaces.

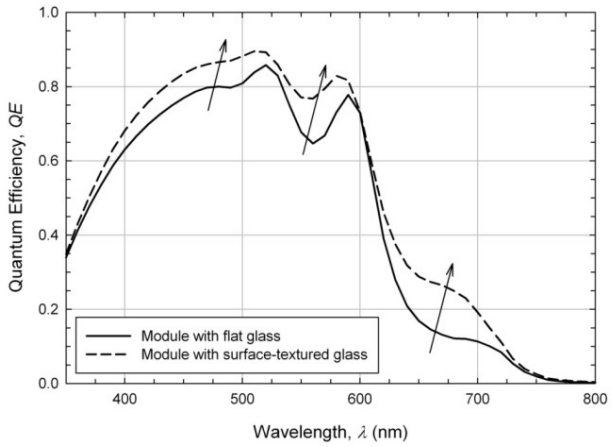

Fig. 6: Simulated quantum efficiency of thin-film a-Si:H solar cell encapsulated with flat (full line) and surface-textured glass (dashed line). CROWM simulator was used in both simulations.

4. Conclusions

An optical model based on the combination of two-dimensional ray tracing and one-dimensional transfer matrix formalism was developed and applied to simulation of thin-film PV devices with thick surface-textured components at the front side. The model was implemented in the CROWM (Combined Ray Optics / Wave Optics Numerical Model) optical simulator. CROWM was verified by means of two established optical simulators based on the scalar scattering theory and the finite element method. In the case of cells with thick surface-textured front components, CROWM shows the potential to greatly reduce the simulation times and thus allows for more efficient analysis of the investigated structures. By means of the developed optical model, *a*-Si:H solar cells with flat interfaces encapsulated with thick flat and surface-textured glass were simulated. The results show that surface-textured protective glass improves light trapping within the thin absorber layers of the solar cell and thus significantly boosts the short-circuit current of the photovoltaic device.

References

/1/ R. E. I. Schropp and M. Zeman, *Amorphous and Microcrystalline Silicon Solar Cells: Modeling, Materials and Device Technology*, 1st ed. Springer, 1998.

/2/ J. Meier et al., "Potential of amorphous and microcrystalline silicon solar cells," *Thin Solid Films*, vol. 451-452, pp. 518-524, 2004.

/3/ L. Ley, "Photoemission and optical properties," in *The Physics of Hydrogenated Amorphous Silicon II*, vol. 56, J. D. Joannopoulos and G. Lucovsky, Eds. Berlin, Heidelberg: Springer Berlin Heidelberg, 1984, pp. 61-168.

/4/ A. V. Shah et al., "Basic efficiency limits, recent experimental results and novel light-trapping schemes in a-Si:H, µc-Si:H and 'micromorph tandem' solar cells," *Journal of Non-Crystalline Solids*, vol. 338-340, pp. 639-645, 2004.

/5/ J. Meier et al., "From R&D to Large-Area Modules at Oerlikon Solar," *MRS Online Proceedings Library*, vol. 1245, 2010.

/6/ M. Schiavoni, P. Gayout, N.-P. Harder, and U. Blieske, "Textured plate comprising asymmetrical patterns," *Patent application*, WO2007015019, 2007.

/7/ J. Krč, F. Smole, and M. Topič, "Analysis of light scattering in amorphous Si:H solar cells by a one-dimensional semi-coherent optical model," *Progress in Photovoltaics: Research and Applications*, vol. 11, no. 1, pp. 15-26, 2003.

/8/ A. Čampa, J. Krč, and M. Topič, "Analysis and optimisation of microcrystalline silicon solar cells with periodic sinusoidal textured interfaces by two-dimensional optical simulations," *Journal of Applied Physics*, vol. 105, no. 8, pp. 083107–083107, 2009.

/9/ C. Haase and H. Stiebig, "Thin-film silicon solar cells with efficient periodic light trapping texture," *Applied Physics Letters*, vol. 91, p. 061116, 2007.

/10/ C. Rockstuhl et al., "Light absorption in textured thin film silicon solar cells: A simple scalar scattering approach versus rigorous simulation," *Applied Physics Letters*, vol. 98, no. 5, p. 051102, 2011.

/11/ B. E. Pieters, J. Krč, and M. Zeman, "Advanced Numerical Simulation Tool for Solar Cells - ASA5," in *Conference Record of the 2006 IEEE 4th World Conference on Photovoltaic Energy Conversion*, 2006, vol. 2, pp. 1513-1516.

/12/ J. Springer, A. Poruba, and M. Vanecek, "Improved three-dimensional optical model for thin-film silicon solar cells," *Journal of Applied Physics*, vol. 96, no. 9, p. 5329, 2004.

/13/ D. Bergström, J. Powell, and A. F. H. Kaplan, "A ray-tracing analysis of the absorption of light by smooth and rough metal surfaces," *Journal of Applied Physics*, vol. 101, p. 113504, 2007.

/14/ R. J. Martin-Palma, J. M. Martinez-Duart, and A. Macleod, "Determination of the optical constants of a semiconductor thin filmemploying the matrix method," *IEEE Transactions on Education*, vol. 43, no. 1, pp. 63-68, 2000.

/15/ M. Born and E. Wolf, *Principles of Optics: Electromagnetic Theory of Propagation, Interference and Diffraction of Light*, 7th ed. Cambridge University Press, 1999.

Benjamin Lipovšek, Janez Krč, Marko Topič
University of Ljubljana, Faculty of Electrical Engineering, Tržaška 25, 1000 Ljubljana, Slovenia
(corresponding e-mail: benjamin.lipovsek@fe.uni-lj.si)

Prispelo: 20.06.2011 *Sprejeto: 24.11.2011*